Quantum quenches and competing orders: I. Time-dependent Hartree-Fock+BCS theory

Wenbo Fu, Ling-Yan Hung, and Subir Sachdev

Department of Physics, Harvard University, Cambridge, MA 02138, USA

(Dated: February 2, 2022)

Abstract

We study the non-equlibrium dynamics of an electronic model of competing bond density wave order and d-wave superconductivity. In a time-dependent Hartree-Fock+BCS approximation, the dynamics reduces to the equations of motion of operators realizing the generators of SU(4) at each pair of momenta, $(\boldsymbol{k}, -\boldsymbol{k})$, in the Brillouin zone. We compare the results of numerical studies of our model with recent picosecond optical experiments.

I. INTRODUCTION

A remarkable series of recent optical experiments[1–4] have explored time-dependent non-equilibrium physics in the cuprate superconductors at the picosecond time scale. Our work is specifically motivated by the observations of Ref. 1: these experiments observed terahertz oscillations in the reflectivity of underdoped of YBCO in a time-domain, pump-probe experiment. The onset temperature of the reflectivity oscillations was the same as the onset temperature of charge ordering in the recent X-ray measurements,[5–7] and so the oscillations were interpreted[1] as an oscillation in the amplitude of the charge order. The reflectivity oscillations also showed an interesting phase shift and temperature-dependent frequency across the superconducting critical temperature T_c, and the authors interpreted these phenomena in a classical phenomenological model of competition between superconductivity and charge order.

Our purpose here, and in the companion paper,[8] is to develop a quantum theory of the oscillations, and to study a Hamiltonian model of the dynamics of competing orders. The present paper will use a simple electronic 'hot-spot' model of the competition between charge order and superconductivity which was proposed recently in Ref. 9. We will extend the equilibrium results to time-dependent phenomena using a time-dependent Hartree-Fock-BCS theory similar to that used in Ref. 10 for the quench dynamics of BCS superconductors. In the second paper,[8] we will use a quantum non-linear sigma model of the competing orders, which is a quantum generalization of the theory proposed in Ref. 11.

II. HOT SPOT MODEL

We begin by reviewing the equilibrium properties of the simple "hot spot" model of competing orders presented in Ref. 9. The model is defined in terms of 4 species of fermions $\Psi_{a\alpha}$, $a = 1 \ldots 4$, $\alpha = \uparrow, \downarrow$ located near "hotspots" on the Fermi surface as shown in Fig. 1. Their kinetic energy is given by

$$H_0 = \sum_{\boldsymbol{k}} \Big[\epsilon_1(\boldsymbol{k})\, \Psi^\dagger_{1\alpha}(\boldsymbol{k}) \Psi_{1\alpha}(\boldsymbol{k}) + \epsilon_2(\boldsymbol{k})\, \Psi^\dagger_{2\alpha}(\boldsymbol{k}) \Psi_{2\alpha}(\boldsymbol{k}) + \epsilon_1(-\boldsymbol{k})\, \Psi^\dagger_{3\alpha}(\boldsymbol{k}) \Psi_{3\alpha}(\boldsymbol{k}) + \epsilon_2(-\boldsymbol{k})\, \Psi^\dagger_{4\alpha}(\boldsymbol{k}) \Psi_{4\alpha}(\boldsymbol{k}) \Big]. \tag{1}$$

We take the origin of momentum space at the hot spots, and orient the x-axis orthogonal to the Fermi surface for the $\Psi_{1,3}$ fermions; so we can write

$$\epsilon_1(\boldsymbol{k}) = k_x + \gamma k_y^2. \tag{2}$$

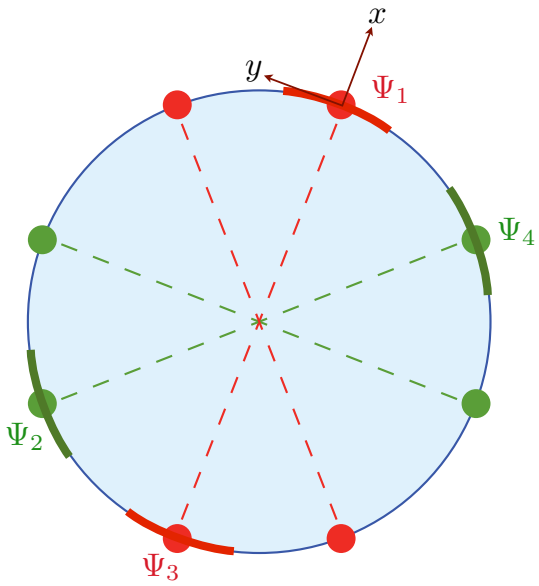

FIG. 1. Definitions of the $\Psi_{1,2,3,4}$ fermions around the Fermi surface. Each fermion resides around a curved patch of the Fermi surface shown by the thick lines. The red (green) hot spots are where the superconducting and bond density wave orders are positive (negative).

We have taken the Fermi velocity to be unit, while γ measures the curvature of the Fermi surface. The dispersion $\epsilon_2(\boldsymbol{k})$ has the form obtained by rotating $\epsilon_1(\boldsymbol{k})$ so that the direction orthogonal to the Fermi surfaces of the $\Psi_{2,4}$ has a linear dispersion. After rescaling momenta appropriately, we can chose the convenient momentum space cutoffs $-\pi < k_x, k_y < \pi$, and the value $\gamma = 1/\pi$.

Next, we add interactions between these fermions. The microscopic exchange (J) interactions and Coulomb repulsion (V) when projected onto the hot spots lead to

$$\begin{aligned} H_1 = \int d^2x \Big[& -J \left(\Psi^\dagger_{1\alpha} \vec{\sigma}_{\alpha\beta} \Psi_{2\beta} + \Psi^\dagger_{2\alpha} \vec{\sigma}_{\alpha\beta} \Psi_{1\beta} \right) \\ & \cdot \left(\Psi^\dagger_{3\gamma} \vec{\sigma}_{\gamma\delta} \Psi_{4\delta} + \Psi^\dagger_{4\gamma} \vec{\sigma}_{\gamma\delta} \Psi_{3\delta} \right) \\ & -V \left(\Psi^\dagger_{1\alpha} \Psi_{2\alpha} + \Psi^\dagger_{2\alpha} \Psi_{1\alpha} \right) \left(\Psi^\dagger_{3\beta} \Psi_{4\beta} + \Psi^\dagger_{4\beta} \Psi_{3\beta} \right) \Big] \end{aligned} \tag{3}$$

The full Hamiltonian $H_0 + H_1$ has an exact SU(2)×SU(2) pseudospin rotation symmetry[12] when $\gamma = 0$ and $V = 0$.

Next, we review the Hartree-Fock-BCS theory of the hotspot model $H_0 + H_1$. The superconducting (SC) order parameter, Δ, involves pairing of particles on antipodal points on the Fermi surface, while the charge density wave (CDW) order, Π, involves pairing of particles with holes on

the antipodal point.[9]

$$\Delta_1(\boldsymbol{k}) = \left\langle \varepsilon_{\alpha\beta}\Psi^\dagger_{1\alpha}(\boldsymbol{k})\Psi^\dagger_{3\beta}(-\boldsymbol{k})\right\rangle \quad ; \quad \Delta_1 \equiv \sum_{\boldsymbol{k}} \Delta_1(\boldsymbol{k})$$
$$\Delta_2(\boldsymbol{k}) = \left\langle \varepsilon_{\alpha\beta}\Psi^\dagger_{2\alpha}(\boldsymbol{k})\Psi^\dagger_{4\beta}(-\boldsymbol{k})\right\rangle \quad ; \quad \Delta_2 \equiv \sum_{\boldsymbol{k}} \Delta_2(\boldsymbol{k})$$
$$\Pi_1(\boldsymbol{k}) = \left\langle \Psi^\dagger_{1\alpha}(\boldsymbol{k})\Psi_{3\alpha}(\boldsymbol{k})\right\rangle \quad ; \quad \Pi_1 \equiv \sum_{\boldsymbol{k}} \Pi_1(\boldsymbol{k})$$
$$\Pi_2(\boldsymbol{k}) = \left\langle \Psi^\dagger_{2\alpha}(\boldsymbol{k})\Psi_{4\alpha}(\boldsymbol{k})\right\rangle \quad ; \quad \Pi_2 \equiv \sum_{\boldsymbol{k}} \Pi_2(\boldsymbol{k}) \tag{4}$$

It was found[9] that optimal state has a d-wave signature for both the superconducting and charge orders, with $\Delta_1 = -\Delta_2$ and $\Pi_1 = -\Pi_2$. For the charge order, this d-wave structure implies that the charge modulation is primarily on the *bonds* of the underlying lattice.[13] With the above orders, the mean field Hamiltonian is

$$\begin{aligned} H_{MF} = H_0 + \frac{(3J-V)}{2}\Big(&-\Delta_1\,\varepsilon_{\alpha\beta}\Psi_{2\alpha}(\boldsymbol{k})\Psi_{4\beta}(-\boldsymbol{k}) \\ &+\Delta_2^*\,\varepsilon_{\alpha\beta}\Psi^\dagger_{1\alpha}(\boldsymbol{k})\Psi^\dagger_{3\beta}(-\boldsymbol{k}) - \Delta_2\,\varepsilon_{\alpha\beta}\Psi_{1\alpha}(\boldsymbol{k})\Psi_{3\beta}(-\boldsymbol{k}) \\ &+\Delta_1^*\,\varepsilon_{\alpha\beta}\Psi^\dagger_{2\alpha}(\boldsymbol{k})\Psi^\dagger_{4\beta}(-\boldsymbol{k})\Big) \\ +\frac{(3J+V)}{2}\Big(&\Pi_1\,\Psi^\dagger_{4\alpha}(\boldsymbol{k})\Psi_{2\alpha}(\boldsymbol{k}) + \Pi_2^*\,\Psi^\dagger_{1\alpha}(\boldsymbol{k})\Psi_{3\alpha}(\boldsymbol{k}) \\ &+\Pi_2\,\Psi^\dagger_{3\alpha}(\boldsymbol{k})\Psi_{1\alpha}(\boldsymbol{k}) + \Pi_1^*\,\Psi^\dagger_{2\alpha}(\boldsymbol{k})\Psi_{4\alpha}(\boldsymbol{k})\Big)\,. \end{aligned} \tag{5}$$

Ref. 9 presented the solution of the equilibrium properties of the Hartree-Fock-BCS equations for a variety of values of J and V. Here, we reproduce in Fig. 2 the solution at one set of parameter values to illustrate the basic temperature dependence of the mean-field order parameters. Note that the CDW order, Π_1 has an onset at a higher T. However, at the superconducting T_c, it starts 'competing' for the Fermi surface with the SC order Δ_1, and so decreases with decreasing T.

III. EQUATIONS OF MOTION

We will follow the same general strategy as in Ref. 10: we will work with Heisenberg equations of motion from the Hamiltonian H_{MF}, where the mean field order parameters Δ_1 and Π_1 take their instantaneous average values.

An important feature of this method for the present model is that that commutators of the operators $\Delta_1(\boldsymbol{k})$ and $\Pi_1(\boldsymbol{k})$ with H_{MF} do not close among themselves: they produce additional operators whose equations of motion we have to also consider. By repeatedly evaluating commu-

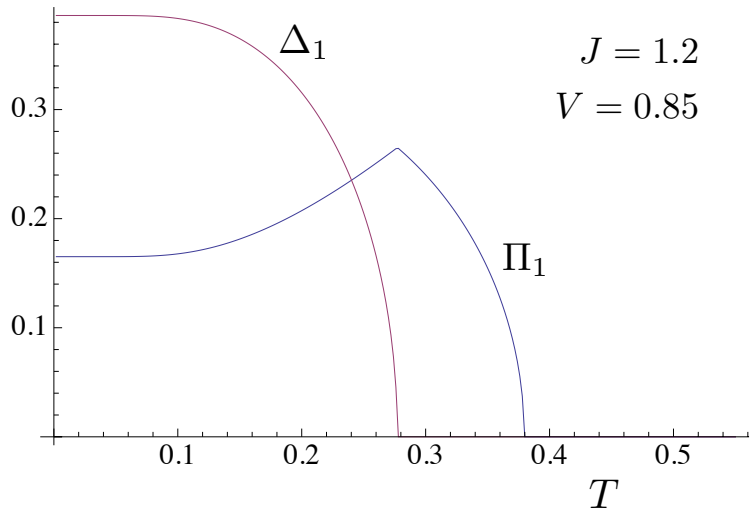

FIG. 2. Superconducting (Δ_1) and bond (Π_1) orders in the hot spot model as a function of T.

tators of the operators so generated, we find that we also have to consider the operators

$$N_i(\boldsymbol{k}) = \Psi^\dagger_{i\alpha}(\boldsymbol{k})\Psi_{i\alpha}(\boldsymbol{k}) \quad , \quad P_i(\boldsymbol{k}) = \varepsilon_{\alpha\beta}\Psi^\dagger_{i\alpha}(\boldsymbol{k})\Psi^\dagger_{i\beta}(-\boldsymbol{k}) \tag{6}$$

where $i = 1 \ldots 4$; note

$$P_i(-\boldsymbol{k}) = P_i(\boldsymbol{k}) \quad , \quad N_i^\dagger(\boldsymbol{k}) = N_i(\boldsymbol{k}). \tag{7}$$

Among all the operators introduced so far, the operator

$$N_1(\boldsymbol{k}) + N_3(\boldsymbol{k}) - N_1(-\boldsymbol{k}) - N_3(-\boldsymbol{k}) \tag{8}$$

commutes with all other operators. The remaining 15 operators

$$\begin{aligned}
&N_1(\boldsymbol{k}) + N_3(-\boldsymbol{k}), N_1(\boldsymbol{k}) + N_1(-\boldsymbol{k}) - 1, N_3(\boldsymbol{k}) + N_3(-\boldsymbol{k}) - 1, \\
&\Delta_1(\boldsymbol{k}), \Delta_1(-\boldsymbol{k}), \Delta_1^\dagger(\boldsymbol{k}), \Delta_1^\dagger(-\boldsymbol{k}), \\
&\Pi_1(\boldsymbol{k}), \Pi_1(-\boldsymbol{k}), \Pi_1^\dagger(\boldsymbol{k}), \Pi_1^\dagger(-\boldsymbol{k}), \\
&P_1(\boldsymbol{k}), P_1^\dagger(\boldsymbol{k}), P_3(\boldsymbol{k}), P_3^\dagger(\boldsymbol{k})
\end{aligned} \tag{9}$$

form the Lie algebra of SU(4). This is to be compared with the SU(2) algebra of Ref. 10 of the operators $P_1(\boldsymbol{k})$, $P_1^\dagger(\boldsymbol{k})$, $N_1(\boldsymbol{k}) + N_1(-\boldsymbol{k}) - 1$.

It is now a straightforward, but tedious, exercise to evaluate the commutators of this SU(4) algebra, and so generate the equations of motion associated with H_{MF}. We display the explicit form of these equations of motion in Appendix A.

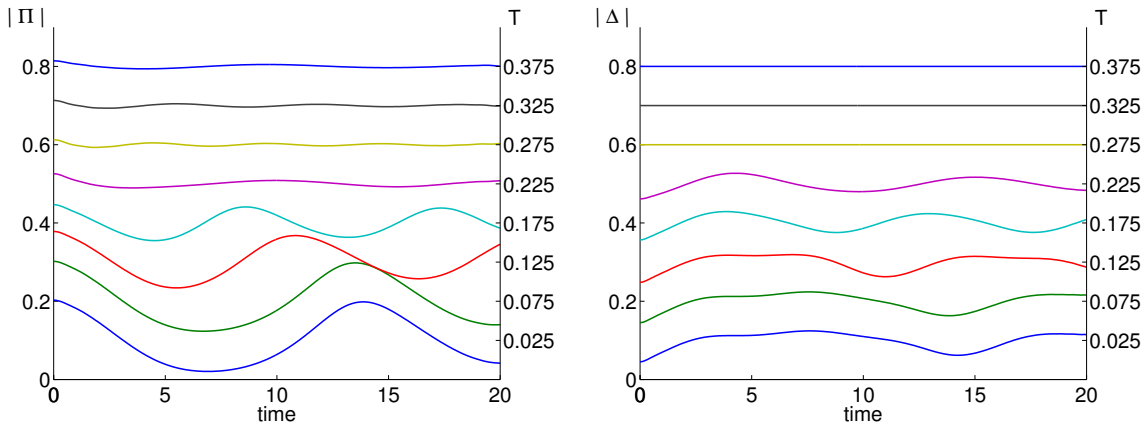

FIG. 3. Oscillation of CDW order parameter Π(left) and SC order parameter Δ(right) as a function of time in the quench case, from low temperature at the bottom to high temperature at the top, temperatures are taken from 0.025 to 0.375 with 0.05 step. Note that here we are plotting the absolute value of the order parameters. Also, we have added constants to the curves to make them evenly spaced. The initial value $J_0 = 1.2$, $V_0 = 0.9$, the quench is taken as $\Delta J = 0, \Delta V = -0.1$. The initial T_c at equilibrium can be computed to be 0.25, the final T_c to be 0.33.

IV. QUENCH

First let us consider the quench case. By quench, we mean the coupling changes abruptly, *i.e.*

$$V(t) = V_0 + \Delta V\,\theta(t) \quad , \quad J(t) = J_0 + \Delta J\,\theta(t) \tag{10}$$

where $\theta(t)$ is the step function, and ΔV and ΔJ are the sizes of the steps. Similar problems have been considered in the BCS system.[10] We take the system to be at equilibrium at the beginning with both CDW and SC order: *i.e.* at a low temperature below the superconducting critical temperature T_c in Fig. 2. The evolutions of order parameters can be obtained using Heisenberg equations of motions. We obtained oscillations of the CDW order parameter Π, and the SC order parameter Δ as a function of time at different temperatures, as shown in Fig. 3 for the parameters $J_0 = 1.2, V_0 = 0.9$, $\Delta J = 0, \Delta V = -0.1$. In the right panel, $|\Delta|$ stays constant because the corresponding temperature is larger than the initial equilibrium T_c; the amplitude of oscillation of the CDW order parameter is also suppressed at high temperature as shown in the left panel.

We fit the data of the CDW order parameter in Fig. 3 by a decayed sinusoidal function Eq. 11.

$$f(t) = ae^{-bt}\sin(ct + d) + e \tag{11}$$

The fit is shown in Fig. 4. In Fig. 5, we show the variation of the amplitude a, frequency c,

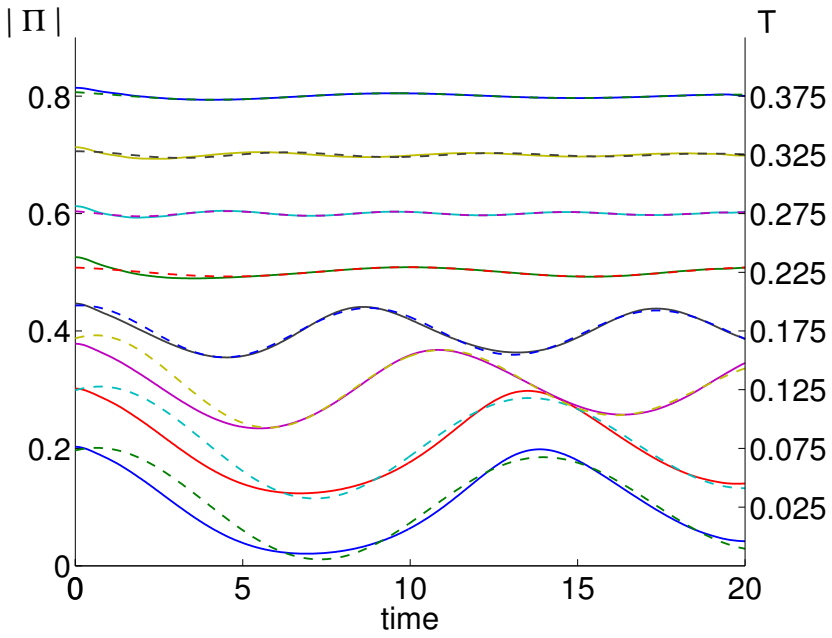

FIG. 4. Fitting of CDW order parameters Π in the left panel of Fig. 3, the dashed lines are fitting lines using $f(t) = ae^{-bt}\sin(ct+d)+e$. We used the data after $time = 5$ and later fittings also obey this rule.

phase d in Eq. 11 as a function of temperature. The most important feature is that the amplitude a is enhanced below the initial T_c at equilibrium, which is also a key feature in the $O(6)$ field theory description.[8] This resembles the oscillatory behavior in the experiment Ref. 1. Also the frequency varies against temperature, and there is a phase shift in the oscillations upon crossing T_c. However, because the frequency changes significantly with temperature, the value of the phase shift is highly dependent upon where we set the onset of oscillations; *i.e.* if we choose our fit function to be $f(t) = ae^{-b(t-t_0)}\sin(c(t-t_0)+d)+e$ the phase shift depends upon t_0. Eq. 11 is actually the choice of $t_0 = 0$, and the phase shift is smaller than π. However, we will see below in Section V that if we choose t_0 appropriately, we can find a nearly π phase shift in the pulse case.

We also note that above T_c, we have $\Delta = 0$, and the mean-field Hamiltonian reduces to

$$H_{MF} = H_0 + \frac{(3J+V)}{2}\Big(\Pi_1\,\Psi^\dagger_{4\alpha}(\boldsymbol{k})\Psi_{2\alpha}(\boldsymbol{k}) + \Pi_2^*\,\Psi^\dagger_{1\alpha}(\boldsymbol{k})\Psi_{3\alpha}(\boldsymbol{k}) \\ +\Pi_2\,\Psi^\dagger_{3\alpha}(\boldsymbol{k})\Psi_{1\alpha}(\boldsymbol{k}) + \Pi_1^*\,\Psi^\dagger_{2\alpha}(\boldsymbol{k})\Psi_{4\alpha}(\boldsymbol{k})\Big)\,. \tag{12}$$

From the commutation relations in Eq. (A1), we can make the identification

$$\Pi_1 \to S_+, \Pi_1^\dagger \to S_-, \frac{N_1 - N_3}{2} \to S_z \tag{13}$$

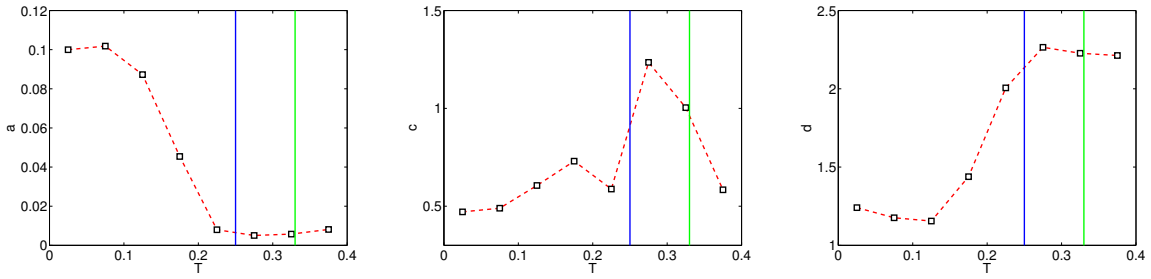

FIG. 5. Left to right: amplitude a, frequency c and phase d of the fit $f(t) = ae^{-bt}\sin(ct+d)+e$ fitting the data in Fig. 4 as a function of temperature. The blue line denotes initial equilibrium $T_c = 0.25$, the green line denotes after quench, the equilibrium $T_c = 0.33$.

Furthermore if we ignore the curvature of the Fermi surface, then $\epsilon_1(\boldsymbol{k}) = -\epsilon_1(-\boldsymbol{k})$, the above Hamiltonian becomes

$$H_{MF} = \sum_{\boldsymbol{k}} \left[2\epsilon_1(\boldsymbol{k}) S_z(\boldsymbol{k}) + \frac{3J+V}{2} \left(-\langle S_- \rangle S_+(\boldsymbol{k}) - \langle S_+ \rangle S_-(\boldsymbol{k}) \right) \right] \tag{14}$$

here we have used $\Pi_2 = -\Pi_1$ and only considered $1,3$ hotspot field (the $2,4$ channel would be similar). And this resembles the well-known pseudospin formulation of the BCS system, as studied in Ref. 10. For a small deviation, the frequency would be proportional to the order parameter Π. This explains the fact that the oscillation frequency decrease rapidly above T_c, and in the same region Π also decreases rapidly with increasing temperature.

We have also computed the positive quench case in Fig. 6, where $J_0 = 1.2, V_0 = 0.9$, $\Delta J = 0, \Delta V = 0.1$. However, here the enhancement of the oscillation amplitude below T_c is not that large.

V. PULSE

Since in the experiment,[1–4] the disturbance is a short-time optical pulse, it should be more reasonable to consider the pulse in our time-dependent Hamiltonian, *i.e.*

$$J(t) = J_0 + \Delta J \left(1 - \tanh^2(\omega t)\right) \quad , \quad V(t) = V_0 + \Delta V \left(1 - \tanh^2(\omega t)\right) \tag{15}$$

We will choose $\omega = 1$. Fig. 7 shows the oscillation when $J_0 = 1.2, V_0 = 0.9$, $\Delta J = 0, \Delta V = -0.1$.

We find similar behavior as in the quench case. We fit the data of the CDW order parameter in Fig. 7 by the same function Eq. 11, as shown in Fig. 8. And Fig. 9 shows the variation of the amplitude a, frequency c, phase d in Eq. 11 as a function of temperature. Here we also have

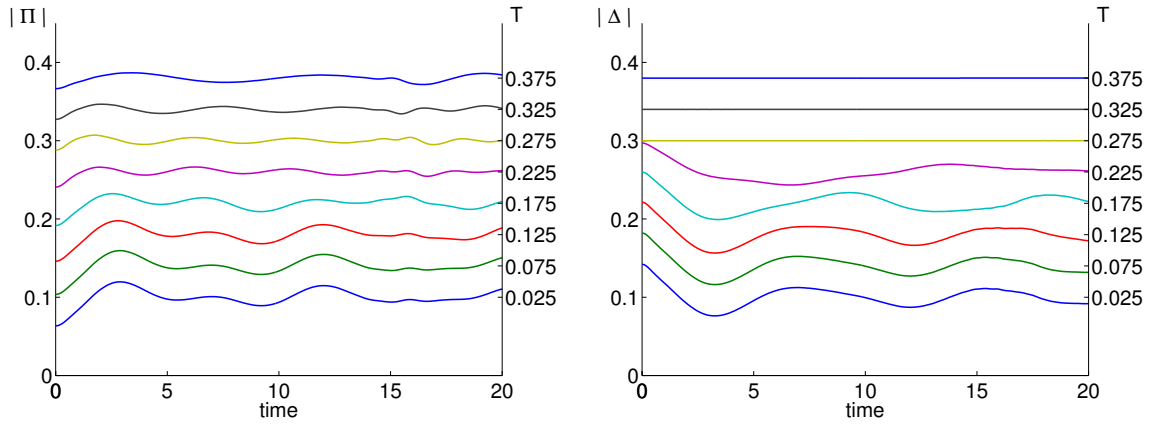

FIG. 6. Oscillation of CDW order parameter Π(left) and SC order parameter Δ(right) as a function of time in the quench case, from low temperature at the bottom to high temperature at the top, temperatures are taken from 0.025 to 0.375 with 0.05 step. Note that here we are plotting the absolute value of the order parameters. The initial value $J_0 = 1.2$, $V_0 = 0.9$, the quench is taken as $\Delta J = 0, \Delta V = -0.1$. The initial T_c at equilibrium can be computed to be 0.25, the final T_c to be 0.2.

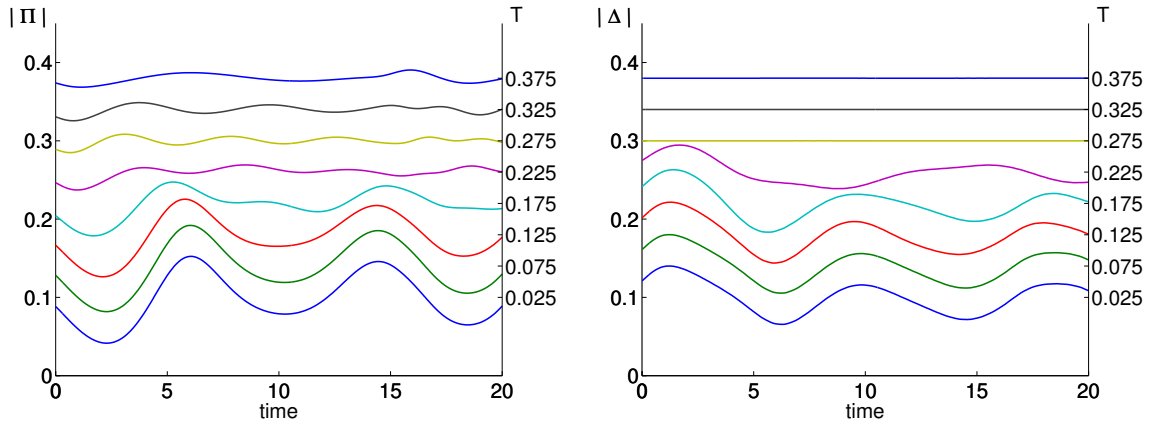

FIG. 7. Oscillation of CDW order parameter Π(left) and SC order parameter Δ(right) as a function of time in the pulse case, from low temperature at the bottom to high temperature at the top, temperatures are taken from 0.025 to 0.375 with 0.05 step. Note that here we are plotting the absolute value of the order parameters. The initial value $J_0 = 1.2$, $V_0 = 0.9$, the pulse is taken as $\Delta J = 0, \Delta V = -0.1$. The initial T_c at equilibrium can be computed to be 0.25, at the largest derivation $V = V_0 + \Delta V$, the corresponding equilibrium T_c to be 0.33.

amplitude enhancement below T_c, frequency's dependence on temperature and phase shift crossing T_c.

As we mentioned before, the phase shift is highly dependent upon where we choose our phase zero point. But in the pulse case, shown in the left panel of Fig. 7, at around time $t = 5.5$, the

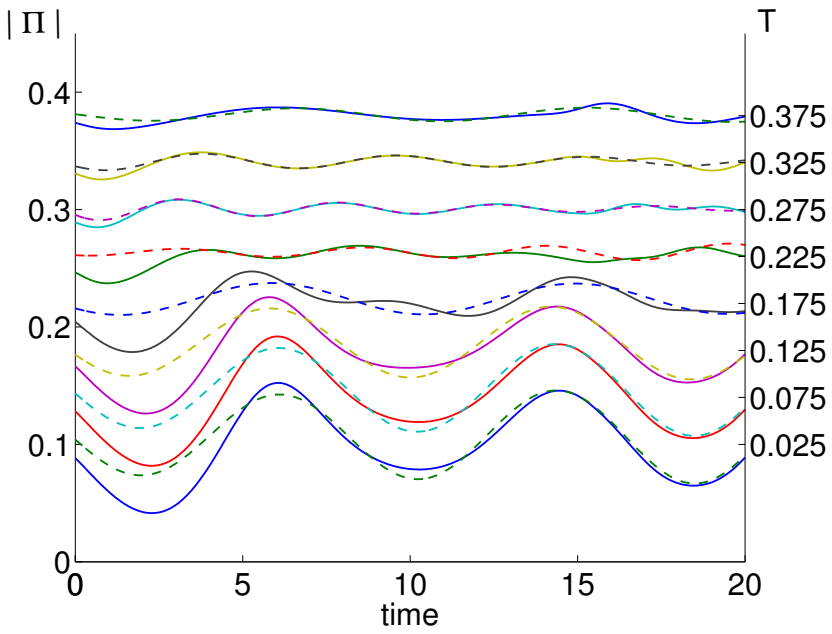

FIG. 8. Fitting of CDW order parameters Π in the left panel of Fig. 7, the dashed lines are fitting lines using $f(t) = ae^{-bt}\sin(ct + d) + e$.

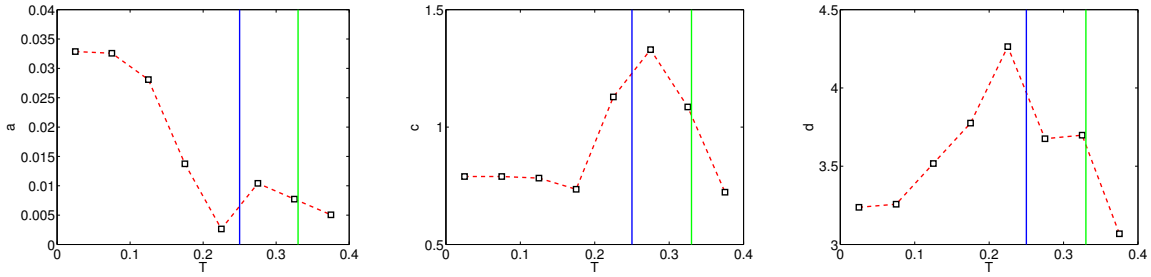

FIG. 9. Left to right: amplitude a, frequency c and phase d of the fit $f(t) = ae^{-bt}\sin(ct + d) + e$ fitting the data in Fig. 8 as a function of temperature. The blue line denotes initial equilibrium $T_c = 0.25$,the green line denotes at the largest derivation $V = V_0 + \Delta V$, the equilibrium $T_c = 0.33$.

first peak at low temperature becomes a valley upon crossing T_c. One can also reach the same conclusion from the fit using $f(t) = ae^{-b(t-t_0)}\sin(c(t - t_0) + d) + e$ as shown in Fig. 10, where $t_0 = 5.5$. The right panel shows the phase is shift around π, as the optical experiment.[1]

Moreover, with a positive pulse $\Delta V = 0.1$, Fig. 11 shows the oscillation behavior. Fig. 12 shows the fit using Eq. 11 and the fitting parameters are shown in Fig. 13. Now, the first valley at low temperature becomes a peak upon crossing T_c. Using the fit function $f(t) = ae^{-b(t-5.5)}\sin(c(t - 5.5) + d) + e$, we get the fit data as shown in Fig 14, and there is a nearly π(or $-\pi$) phase shift crossing T_c. Another difference is that with positive pulse, SC paring instability is suppressed,

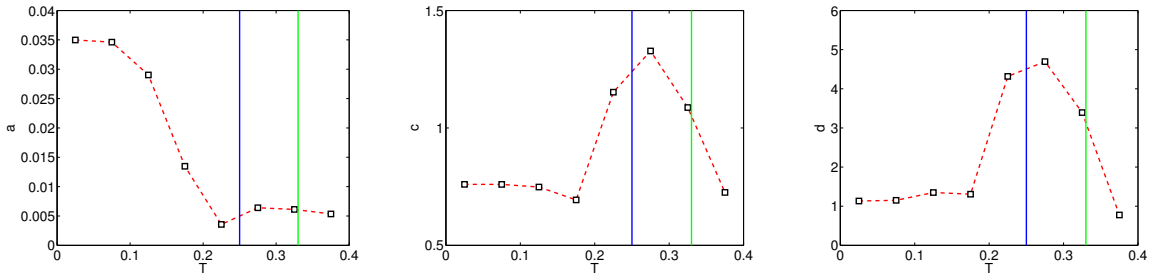

FIG. 10. Left to right: amplitude a, frequency c and phase d of the fit $f(t) = ae^{-b(t-t_0)}\sin(c(t-t_0)+d)+e$ with $t_0 = 5.5$ fitting the data in Fig. 8 as a function of temperature. The blue line denotes initial equilibrium $T_c = 0.25$,the green line denotes at the largest derivation $V = V_0 + \Delta V$, the equilibrium $T_c = 0.33$.

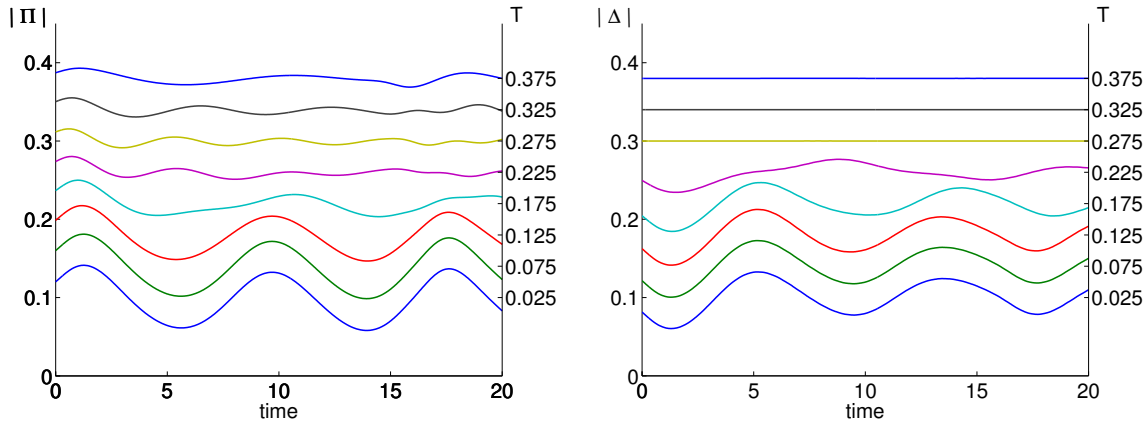

FIG. 11. Oscillation of CDW order parameter Π(left) and SC order parameter Δ(right) as a function of time in the pulse case, from low temperature at the bottom to high temperature at the top, temperatures are taken from 0.025 to 0.375 with 0.05 step. Note that here we are plotting the absolute value of the order parameters. The initial value $J_0 = 1.2$, $V_0 = 0.9$, the quench is taken as $\Delta J = 0, \Delta V = 0.1$. The initial T_c at equilibrium can be computed to be 0.25, at the largest derivation $V = V_0 + \Delta V$, the corresponding equilibrium T_c to be 0.2.

then the enhancement will start at a lower temperature compared to the negative pulse case; this can be seen from the first panel of Fig. 9 and Fig. 13.

Fig. 15 shows a direct comparison of our simulation and the experimental data. Both data indicate enhancement of CDW oscillation below T_c. But the frequency is more dependent on temperature in the numerics than in the experiment, as a result, the phase shift is delicate to define. If we choose our phase starting point $t_0 = 5.5$ in the fit function $f(t) = Ae^{-b(t-t_0)}\sin(\nu(t-t_0)+\Phi)+e$, there will be a nearly π phase shift crossing T_c, but the so-defined phase will not stay unchanged at high temperature because of the large frequency dependence on temperature in the

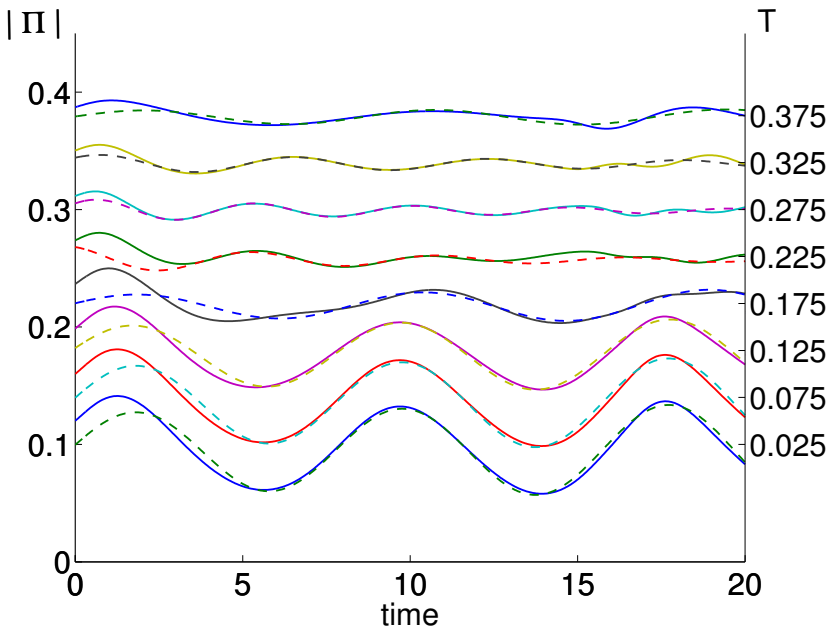

FIG. 12. Fitting of CDW order parameters Π in the left panel of Fig. 11, the dashed lines are fitting lines using $f(t) = ae^{-bt}\sin(ct + d) + e$.

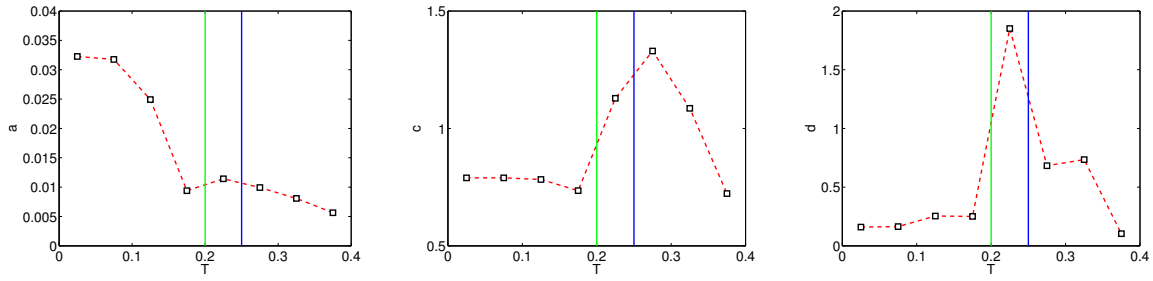

FIG. 13. Left to right: amplitude a, frequency c and phase d of the fit $f(t) = ae^{-bt}\sin(ct + d) + e$ fitting the data in Fig. 12 as a function of temperature. The blue line denotes initial equilibrium $T_c = 0.25$, the green line denotes at the largest derivation $V = V_0 + \Delta V$, the equilibrium $T_c = 0.2$.

numerics.

We also examined the quench or pulse J case, i.e. $\Delta J \neq 0$. In this case, our numerics showed no clear enhancement of oscillation below T_c. We show one case when pulse $\Delta J = 0.1, \Delta V = 0$ in Fig. 16: no obvious enhancement or phase shift is observed crossing T_c.

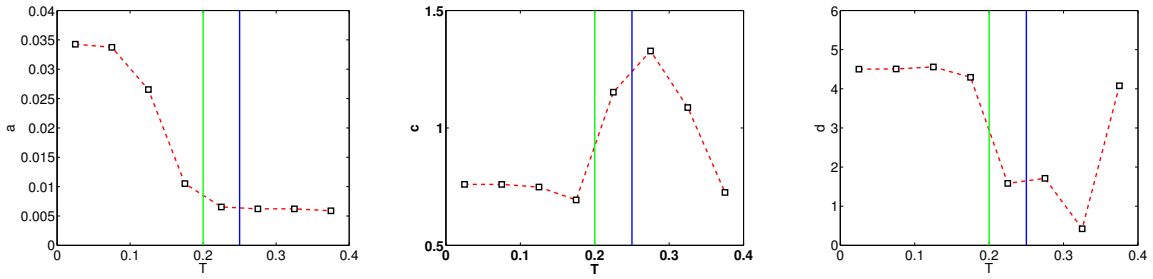

FIG. 14. Left to right: amplitude a, frequency c and phase d of the fit $f(t) = ae^{-b(t-t_0)}\sin(c(t-t_0)+d)+e$ with $t_0 = 5.5$ fitting the data in Fig. 12 as a function of temperature. The blue line denotes initial equilibrium $T_c = 0.25$, the green line denotes at the largest derivation $V = V_0 + \Delta V$, the equilibrium $T_c = 0.2$.

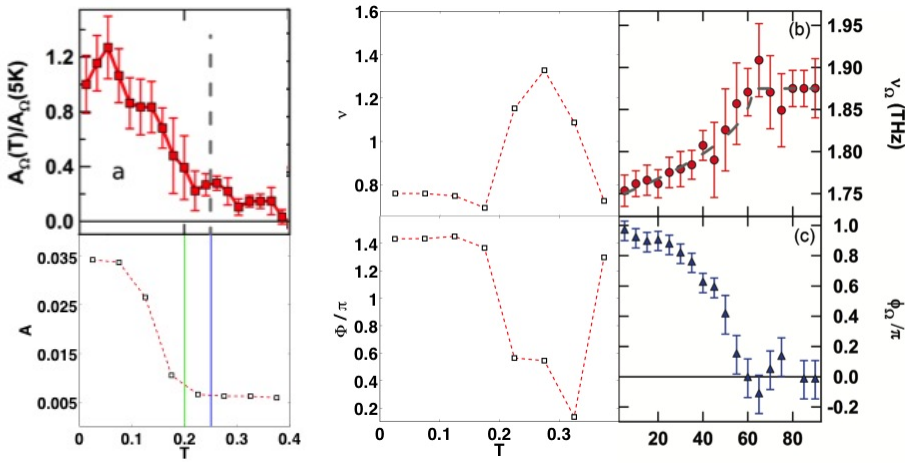

FIG. 15. Comparison of the numerics (dashed red line) from Fig. 14 and experiment data[1](red and blue dots). Left panel is amplitude against temperature, where dashed grey line denotes initial T_c before perturbation in the experiment, the blue line denotes initial T_c in the numerics, the green line denotes the equilibrium T_c at the largest derivation $V = V_0 + \Delta V$ in the numerics. The right penal shows the comparison in frequency and phase.

VI. CONCLUSIONS

Using a time-dependent Hartree-Fock computation, we have studied the non-equilibrium dynamics of SC and CDW order parameters in the t-J-V model.[9] We examined two setups: quench and pulse in the interaction parameters, and compared with a recent optical experiment.[1] We use decayed sinusoidal function to fit the oscillation. When perturbing with the nearest neighbor Coulomb interaction V, we found an enhanced oscillation amplitude of the CDW order below the superconducting critical temperature in both setups. We interpret this enhancement as a compe-

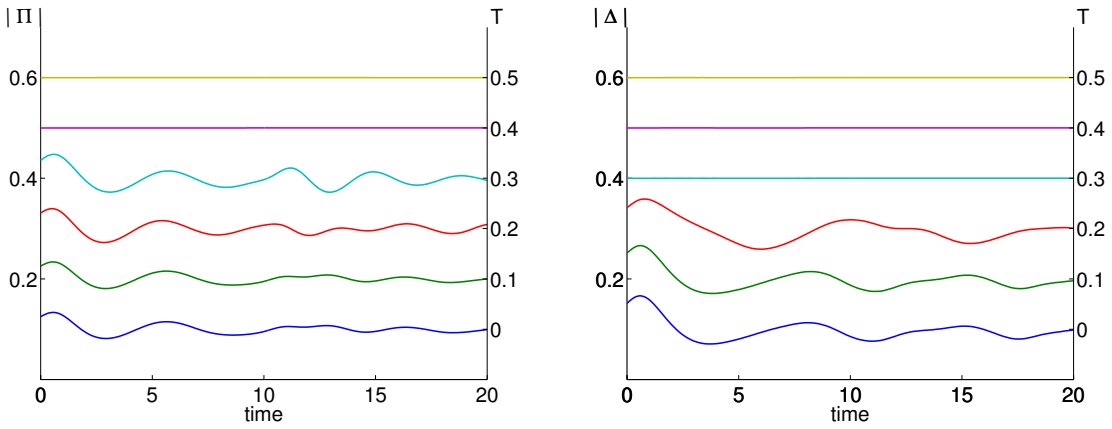

FIG. 16. Oscillation of CDW order parameter Π(left) and SC order parameter Δ(right) as a function of time in the pulse case, from low temperature at the bottom to high temperature at the top, temperatures are taken from 0 to 0.5 with 0.1 step. Note that here we are plotting the absolute value of the order parameters. The initial value $J_0 = 1.2$, $V_0 = 0.9$, the quench is taken as $\Delta J = 0.1, \Delta V = 0$.

tition between the charge order and superconducting order. The frequency of the oscillations also depends on temperature, which makes it subtle to define the relative phase between oscillations at different temperatures. But, if we choose particular phase starting point in the fit function, we find a nearly π phase shift in the pulse case crossing T_c, as observed in the experiments.[1] When perturbing the exchange interaction J, in both setups, there is no obvious enhancement in the oscillation amplitude crossing T_c.

ACKNOWLEDGMENTS

We thank A. Cavelleri, N. Gedik, F. Mahmood, J. Orenstein, and A. Vishwanath for valuable discussions. The research was supported by the U.S. National Science Foundation under grant DMR-1103860, and by the Templeton Foundation. LH was supported by the Croucher foundation.

Appendix A: Equations of motion

It is a simple matter to evaluate the commutators of the operators in Eq. (9):

$$
\begin{aligned}
[N_1(\boldsymbol{k}), \Delta_1(\boldsymbol{k})] &= \Delta_1(\boldsymbol{k}) \\
\left[N_1(\boldsymbol{k}), \Delta_1^\dagger(\boldsymbol{k})\right] &= -\Delta_1^\dagger(\boldsymbol{k}) \\
[N_1(\boldsymbol{k}), \Pi_1(\boldsymbol{k})] &= \Pi_1(\boldsymbol{k}) \\
\left[N_1(\boldsymbol{k}), \Pi_1^\dagger(\boldsymbol{k})\right] &= -\Pi_1^\dagger(\boldsymbol{k}) \\
[N_1(\boldsymbol{k}), P_1(\boldsymbol{k})] &= P_1(\boldsymbol{k}) \\
\left[N_1(\boldsymbol{k}), P_1^\dagger(\boldsymbol{k})\right] &= -P_1^\dagger(\boldsymbol{k}) \\
[N_3(\boldsymbol{k}), \Delta_1(-\boldsymbol{k})] &= \Delta_1(-\boldsymbol{k}) \\
\left[N_3(\boldsymbol{k}), \Delta_1^\dagger(-\boldsymbol{k})\right] &= -\Delta_1^\dagger(-\boldsymbol{k}) \\
[N_3(\boldsymbol{k}), \Pi_1(\boldsymbol{k})] &= -\Pi_1(\boldsymbol{k}) \\
\left[N_3(\boldsymbol{k}), \Pi_1^\dagger(\boldsymbol{k})\right] &= \Pi_1^\dagger(\boldsymbol{k}) \\
[N_3(\boldsymbol{k}), P_3(\boldsymbol{k})] &= P_3(\boldsymbol{k}) \\
\left[N_3(\boldsymbol{k}), P_3^\dagger(\boldsymbol{k})\right] &= -P_3^\dagger(\boldsymbol{k}) \\
\left[\Delta_1(\boldsymbol{k}), \Delta_1^\dagger(\boldsymbol{k})\right] &= N_1(\boldsymbol{k}) + N_3(-\boldsymbol{k}) \\
[\Delta_1(\boldsymbol{k}), \Pi_1(-\boldsymbol{k})] &= -P_1(\boldsymbol{k}) \\
\left[\Delta_1(\boldsymbol{k}), \Pi_1^\dagger(\boldsymbol{k})\right] &= -P_3(\boldsymbol{k}) \\
\left[\Delta_1(\boldsymbol{k}), P_1^\dagger(\boldsymbol{k})\right] &= \Pi_1^\dagger(-\boldsymbol{k}) \\
\left[\Delta_1(\boldsymbol{k}), P_3^\dagger(\boldsymbol{k})\right] &= \Pi_1(\boldsymbol{k}) \\
\left[\Pi_1(\boldsymbol{k}), \Pi_1^\dagger(\boldsymbol{k})\right] &= N_1(\boldsymbol{k}) - N_3(\boldsymbol{k}) \\
\left[\Pi_1(\boldsymbol{k}), P_1^\dagger(\boldsymbol{k})\right] &= -\Delta_1^\dagger(-\boldsymbol{k}) \\
[\Pi_1(\boldsymbol{k}), P_3(\boldsymbol{k})] &= \Delta_1(\boldsymbol{k}) \\
\left[P_1(\boldsymbol{k}), P_1^\dagger(\boldsymbol{k})\right] &= N_1(\boldsymbol{k}) + N_1(-\boldsymbol{k}) - 1 \\
\left[P_3(\boldsymbol{k}), P_3^\dagger(\boldsymbol{k})\right] &= N_3(\boldsymbol{k}) + N_3(-\boldsymbol{k}) - 1
\end{aligned}
\tag{A1}
$$

and some others that follow under $\boldsymbol{k} \to -\boldsymbol{k}$ and/or Hermitian conjugates.

A similar set of relations follow from $1 \to 2$ and $3 \to 4$, yielding a second SU(4) algebra. However, we will not need these because we will always assume $\Delta_2 = -\Delta_1$ and $\Pi_2 = -\Pi_1$.

Then we can use H_{MF} in Eq. (5) to obtain the equations of motion of the average values of the

operators in Eq. (9):

$$
\begin{aligned}
\frac{d\Delta_1(\boldsymbol{k})}{dt} &= -i\left[-\epsilon_1(\boldsymbol{k})\Delta_1(\boldsymbol{k}) - \epsilon_1(\boldsymbol{k})\Delta_1(\boldsymbol{k}) + \frac{(3J-V)}{2}\Delta_2(N_1(\boldsymbol{k}) + N_3(-\boldsymbol{k})) + \frac{3J+V}{2}(-\Pi_2^* P_1(\boldsymbol{k}) - \Pi_2 P_3(\boldsymbol{k}))\right] \\
\frac{d\Delta_1(-\boldsymbol{k})}{dt} &= -i\left[-\epsilon_1(-\boldsymbol{k})\Delta_1(-\boldsymbol{k}) - \epsilon_1(-\boldsymbol{k})\Delta_1(-\boldsymbol{k}) + \frac{(3J-V)}{2}\Delta_2(N_1(-\boldsymbol{k}) + N_3(\boldsymbol{k})) + \frac{3J+V}{2}(-\Pi_2^* P_1(\boldsymbol{k}) - \Pi_2 P_3(\boldsymbol{k}))\right] \\
\frac{d\Delta_1^\dagger(\boldsymbol{k})}{dt} &= -i\left[\epsilon_1(\boldsymbol{k})\Delta_1^\dagger(\boldsymbol{k}) + \epsilon_1(\boldsymbol{k})\Delta_1^\dagger(\boldsymbol{k}) - \frac{(3J-V)}{2}\Delta_2^*(N_1(\boldsymbol{k}) + N_3(-\boldsymbol{k})) - \frac{3J+V}{2}(-\Pi_2 P_1^\dagger(\boldsymbol{k}) - \Pi_2^* P_3^\dagger(\boldsymbol{k}))\right] \\
\frac{d\Delta_1^\dagger(-\boldsymbol{k})}{dt} &= -i\left[\epsilon_1(-\boldsymbol{k})\Delta_1^\dagger(-\boldsymbol{k}) + \epsilon_1(-\boldsymbol{k})\Delta_1^\dagger(-\boldsymbol{k}) - \frac{(3J-V)}{2}\Delta_2^*(N_1(-\boldsymbol{k}) + N_3(\boldsymbol{k})) - \frac{3J+V}{2}(-\Pi_2 P_1^\dagger(\boldsymbol{k}) - \Pi_2^* P_3^\dagger(\boldsymbol{k}))\right] \\
\frac{d\Pi_1(\boldsymbol{k})}{dt} &= -i\left[-\epsilon_1(\boldsymbol{k})\Pi_1(\boldsymbol{k}) + \epsilon_1(-\boldsymbol{k})\Pi_1(\boldsymbol{k}) + \frac{(3J-V)}{2}(-\Delta_2 P_3^\dagger(\boldsymbol{k}) + \Delta_2^* P_1(\boldsymbol{k})) + \frac{3J+V}{2}\Pi_2(N_1(\boldsymbol{k}) - N_3(\boldsymbol{k}))\right] \\
\frac{d\Pi_1(-\boldsymbol{k})}{dt} &= -i\left[-\epsilon_1(-\boldsymbol{k})\Pi_1(-\boldsymbol{k}) + \epsilon_1(\boldsymbol{k})\Pi_1(-\boldsymbol{k}) + \frac{(3J-V)}{2}(-\Delta_2 P_3^\dagger(\boldsymbol{k}) + \Delta_2^* P_1(\boldsymbol{k})) + \frac{3J+V}{2}\Pi_2(N_1(-\boldsymbol{k}) - N_3(-\boldsymbol{k}))\right] \\
\frac{d\Pi_1^\dagger(\boldsymbol{k})}{dt} &= -i\left[\epsilon_1(\boldsymbol{k})\Pi_1^\dagger(\boldsymbol{k}) - \epsilon_1(-\boldsymbol{k})\Pi_1^\dagger(\boldsymbol{k}) - \frac{(3J-V)}{2}(-\Delta_2^* P_3(\boldsymbol{k}) + \Delta_2 P_1^\dagger(\boldsymbol{k})) - \frac{3J+V}{2}\Pi_2^*(N_1(\boldsymbol{k}) - N_3(\boldsymbol{k}))\right] \\
\frac{d\Pi_1^\dagger(-\boldsymbol{k})}{dt} &= -i\left[\epsilon_1(-\boldsymbol{k})\Pi_1^\dagger(-\boldsymbol{k}) - \epsilon_1(\boldsymbol{k})\Pi_1^\dagger(-\boldsymbol{k}) - \frac{(3J-V)}{2}(-\Delta_2^* P_3(\boldsymbol{k}) + \Delta_2 P_1^\dagger(\boldsymbol{k})) - \frac{3J+V}{2}\Pi_2^*(N_1(-\boldsymbol{k}) - N_3(-\boldsymbol{k}))\right] \\
\frac{dP_1(\boldsymbol{k})}{dt} &= -i\left[-(\epsilon_1(\boldsymbol{k}) + \epsilon_1(-\boldsymbol{k}))P_1(\boldsymbol{k}) + \frac{(3J-V)}{2}\Delta_2(\Pi_1(-\boldsymbol{k}) + \Pi_1(\boldsymbol{k})) - \frac{3J+V}{2}\Pi_2(\Delta_1(-\boldsymbol{k}) + \Delta_1(\boldsymbol{k}))\right] \\
\frac{dP_1^\dagger(\boldsymbol{k})}{dt} &= -i\left[(\epsilon_1(\boldsymbol{k}) + \epsilon_1(-\boldsymbol{k}))P_1^\dagger(\boldsymbol{k}) - \frac{(3J-V)}{2}\Delta_2^*(\Pi_1^\dagger(-\boldsymbol{k}) + \Pi_1^\dagger(\boldsymbol{k})) + \frac{3J+V}{2}\Pi_2^*(\Delta_1^\dagger(-\boldsymbol{k}) + \Delta_1^\dagger(\boldsymbol{k}))\right] \\
\frac{dP_3(\boldsymbol{k})}{dt} &= -i\left[-(\epsilon_1(-\boldsymbol{k}) + \epsilon_1(\boldsymbol{k}))P_3(\boldsymbol{k}) + \frac{(3J-V)}{2}\Delta_2(\Pi_1^\dagger(\boldsymbol{k}) + \Pi_1^\dagger(-\boldsymbol{k})) - \frac{3J+V}{2}\Pi_2^*(\Delta_1(\boldsymbol{k}) + \Delta_1(-\boldsymbol{k}))\right] \\
\frac{dP_3^\dagger(\boldsymbol{k})}{dt} &= -i\left[(\epsilon_1(-\boldsymbol{k}) + \epsilon_1(\boldsymbol{k}))P_3^\dagger(\boldsymbol{k}) - \frac{(3J-V)}{2}\Delta_2^*(\Pi_1(\boldsymbol{k}) + \Pi_1(-\boldsymbol{k})) + \frac{3J+V}{2}\Pi_2(\Delta_1^\dagger(\boldsymbol{k}) + \Delta_1^\dagger(-\boldsymbol{k}))\right] \\
\frac{dN_1(\boldsymbol{k})}{dt} &= -i\left[\frac{3J-V}{2}(\Delta_2^*\Delta_1(\boldsymbol{k}) - \Delta_2\Delta_1^\dagger(\boldsymbol{k})) + \frac{3J+V}{2}(\Pi_2^*\Pi_1(\boldsymbol{k}) - \Pi_2\Pi_1^\dagger(\boldsymbol{k}))\right] \\
\frac{dN_1(-\boldsymbol{k})}{dt} &= -i\left[\frac{3J-V}{2}(\Delta_2^*\Delta_1(-\boldsymbol{k}) - \Delta_2\Delta_1^\dagger(-\boldsymbol{k})) + \frac{3J+V}{2}(\Pi_2^*\Pi_1(-\boldsymbol{k}) - \Pi_2\Pi_1^\dagger(-\boldsymbol{k}))\right] \\
\frac{dN_3(\boldsymbol{k})}{dt} &= -i\left[\frac{3J-V}{2}(\Delta_2^*\Delta_1(-\boldsymbol{k}) - \Delta_2\Delta_1^\dagger(-\boldsymbol{k})) + \frac{3J+V}{2}(-\Pi_2^*\Pi_1(\boldsymbol{k}) + \Pi_2\Pi_1^\dagger(\boldsymbol{k}))\right] \\
\frac{dN_3(-\boldsymbol{k})}{dt} &= -i\left[\frac{3J-V}{2}(\Delta_2^*\Delta_1(\boldsymbol{k}) - \Delta_2\Delta_1^\dagger(\boldsymbol{k})) + \frac{3J+V}{2}(-\Pi_2^*\Pi_1(-\boldsymbol{k}) + \Pi_2\Pi_1^\dagger(-\boldsymbol{k}))\right]
\end{aligned}
\tag{A2}
$$

Also note that the operators $P_1 + P_2$ and $P_3 + P_4$ (and their Hermitian conjugates) commute with the original Hamiltonian H for $V = 0$; these operators generate the pseudospin symmetry between the SC and CDW order parameters.

One quality that remains constant during the oscillation is the mean field energy $\langle H_{MF} \rangle$, if the interaction parameters are constant with respect to time, like during the time after the quench. This can be easily verified using Eq. (A2). And this can be used to check the validity of the numerics.

$$\langle H_{MF}\rangle = \sum_{\boldsymbol{k}}\Big[\epsilon_1(\boldsymbol{k})N_1(\boldsymbol{k}) + \epsilon_1(-\boldsymbol{k})N_3(\boldsymbol{k}) + \epsilon_2(\boldsymbol{k})N_2(\boldsymbol{k}) + \epsilon_2(-\boldsymbol{k})N_4(\boldsymbol{k})\Big]$$
$$+\frac{3J-V}{2}\left(\Delta_1\Delta_2^* + \Delta_2\Delta_1^*\right) + \frac{3J+V}{2}\left(\Pi_1\Pi_2^* + \Pi_1^*\Pi_2\right) \tag{A3}$$

Notice that we have added back some subtractions terms to Eq. (5). Then the time derivative of $\langle H_{MF}\rangle$ becomes

$$\begin{aligned}
\frac{1}{2}\frac{d\langle H_{MF}\rangle}{dt} = &\sum_{\boldsymbol{k}} -i\epsilon_1(\boldsymbol{k})\left[\frac{3J-V}{2}(\Delta_2^*\Delta_1(-\boldsymbol{k}) - \Delta_2\Delta_1^\dagger(-\boldsymbol{k})) + \frac{3J+V}{2}(\Pi_2^*\Pi_1(-\boldsymbol{k}) - \Pi_2\Pi_1^\dagger(-\boldsymbol{k}))\right] \\
&- i\epsilon_1(-\boldsymbol{k})\left[\frac{3J-V}{2}(\Delta_2^*\Delta_1(-\boldsymbol{k}) - \Delta_2\Delta_1^\dagger(-\boldsymbol{k})) + \frac{3J+V}{2}(-\Pi_2^*\Pi_1(\boldsymbol{k}) + \Pi_2\Pi_1^\dagger(\boldsymbol{k}))\right] \\
&- i\frac{3J-V}{2}\Delta_2^*\left[-\epsilon_1(\boldsymbol{k})\Delta_1(\boldsymbol{k}) - \epsilon_1(\boldsymbol{k})\Delta_1(\boldsymbol{k}) + \frac{(3J-V)}{2}\Delta_2(N_1(\boldsymbol{k}) + N_3(-\boldsymbol{k})) + \frac{3J+V}{2}(-\Pi_2^*P_1(\boldsymbol{k}) - \Pi_2P_3(\boldsymbol{k}))\right] \\
&- i\frac{3J-V}{2}\Delta_2\left[\epsilon_1(\boldsymbol{k})\Delta_1^*(\boldsymbol{k}) + \epsilon_1(\boldsymbol{k})\Delta_1^*(\boldsymbol{k}) - \frac{(3J-V)}{2}\Delta_2^*(N_1(\boldsymbol{k}) + N_3(-\boldsymbol{k})) - \frac{3J+V}{2}(-\Pi_2P_1^*(\boldsymbol{k}) - \Pi_2^*P_3^*(\boldsymbol{k}))\right] \\
&- i\frac{3J+V}{2}\Pi_2^*\left[-\epsilon_1(\boldsymbol{k})\Pi_1(\boldsymbol{k}) + \epsilon_1(-\boldsymbol{k})\Pi_1(\boldsymbol{k}) + \frac{(3J-V)}{2}(-\Delta_2P_3^*(\boldsymbol{k}) + \Delta_2^*P_1(\boldsymbol{k})) + \frac{3J+V}{2}\Pi_2(N_1(\boldsymbol{k}) - N_3(\boldsymbol{k}))\right] \\
&- i\frac{3J+V}{2}\Pi_2\left[-\epsilon_1(\boldsymbol{k})\Pi_1^*(\boldsymbol{k}) + \epsilon_1(-\boldsymbol{k})\Pi_1^*(\boldsymbol{k}) - \frac{(3J-V)}{2}(-\Delta_2^*P_3(\boldsymbol{k}) + \Delta_2P_1^*(\boldsymbol{k})) - \frac{3J+V}{2}\Pi_2^*(N_1(\boldsymbol{k}) - N_3(\boldsymbol{k}))\right] \\
&= 0
\end{aligned} \tag{A4}$$

where we have assumed time-independence of J and V, which is true in the quench case.

[1] J. P. Hinton, J. D. Koralek, Y. M. Lu, A. Vishwanath, J. Orenstein, D. A. Bonn, W. N. Hardy, and Ruixing Liang, Phys. Rev. B **88**, 060508 (2013).

[2] D. H. Torchinsky, F. Mahmood, A. T. Bollinger, Ivan Božović, and N. Gedik, Nature Materials **12**, 387 (2013).

[3] D. Fausti, R. Tobey, N. Dean, S. Kaiser, A. Dienst, M. Hoffmann, S. Pyon, T. Takayama, H. Takagi, and A. Cavalleri, Science **331**, 189 (2011).

[4] S. Kaiser, D. Nicoletti, C. R. Hunt, W. Hu, I. Gierz, H. Y. Liu, M. Le Tacon, T. Loew, D. Haug, B. Keimer, and A. Cavalleri, arXiv:1205.4661.

[5] G. Ghiringhelli, M. Le Tacon, M. Minola, S. Blanco-Canosa, C. Mazzoli, N. B. Brookes, G. M. De Luca, A. Frano, D. G. Hawthorn, F. He, T. Loew, M. Moretti Sala, D. C. Peets, M. Salluzzo, E. Schierle, R. Sutarto, G. A. Sawatzky, E. Weschke, B. Keimer, and L. Braicovich, Science **337**, 821 (2012).

[6] J. Chang, E. Blackburn, A. T. Holmes, N. B. Christensen, J. Larsen, J. Mesot, Ruixing Liang, D. A. Bonn, W. N. Hardy, A. Watenphul, M. v. Zimmermann, E. M. Forgan, and S. M. Hayden, Nature Phys. **8**, 871 (2012).

[7] A. J. Achkar, R. Sutarto, X. Mao, F. He, A. Frano, S. Blanco-Canosa, M. Le Tacon, G. Ghiringhelli, L. Braicovich, M. Minola, M. Moretti Sala, C. Mazzoli, Ruixing Liang, D. A. Bonn, W. N. Hardy, B. Keimer, G. A. Sawatzky, and D. G. Hawthorn Phys. Rev. Lett. **109**, 167001 (2012).

[8] Ling-Yan Hung, Wenbo Fu, and S. Sachdev, to appear.

[9] J. D. Sau and S. Sachdev, arXiv:1311.3298.

[10] R. A. Barankov and L. S. Levitov, Phys. Rev. Lett. **96**, 230403 (2006).

[11] L. E. Hayward, D. G. Hawthorn, R. G. Melko, and S. Sachdev, arXiv:1309.6639.

[12] M. A. Metlitski and S. Sachdev, Phys. Rev. B **82**, 075128 (2010).

[13] S. Sachdev and R. La Placa, Phys. Rev. Lett. **111**, 027202 (2013).